Catalysis Today 170 (2011) 85–92

Contents lists available at ScienceDirect

Catalysis Today

journal homepage: www.elsevier.com/locate/cattod

Facile synthesis by polyol method of a ruthenium catalyst supported on γ-Al_2O_3 for hydrolytic dehydrogenation of ammonia borane

Giovanni P. Rachiero, Umit B. Demirci*, Philippe Miele

Université Lyon 1, CNRS, UMR 5615, Laboratoire des Multimatériaux et Interfaces, 43 boulevard du 11 Novembre 1918, F-69622 Villeurbanne, France

ARTICLE INFO

Article history:
Received 27 October 2010
Received in revised form 10 January 2011
Accepted 11 January 2011
Available online 24 February 2011

Keywords:
Ammonia borane
Heterogeneous catalysis
Hydrogen storage
Hydrolysis
Ruthenium supported over alumina

ABSTRACT

Ruthenium (1.5 wt% Ru) supported on γ-Al_2O_3 was synthesized in the presence of ethylene glycol using ruthenium acetylacetonate as precursor. The catalyst was characterized by inductively coupled plasma (ICP) emission spectroscopy, X-ray diffraction (XRD), scanning electron microscopy (SEM), transmission electron microscopy (TEM), energy dispersive X-ray (EDX) spectroscopy and X-ray photoelectron spectroscopy (XPS). It was found that it consisted of Ru^0 and RuO_2 as spherical nanoparticles, with an average size of 4.2 nm, and aggregates deposited at the surface of the support. The catalyst was tested in hydrolysis of ammonia borane, NH_3BH_3. Experiments with variable amounts of catalyst (10–30 wt%), concentrations of the substrate (1.0–0.65 M), and temperatures (50–66 °C) were performed. The reaction was followed by volumetric (inverted burette) and spectroscopic (^{11}B and $^{11}B\{^1H\}$ NMR) methods. A kinetic study was developed (apparent activation energy of 67 kJ mol^{-1}; reaction orders *vs.* the concentration of NH_3BH_3 and ruthenium active sites of 0.4 and 1.0, respectively). Hydrogen generation rates up to 76.4 mL(H_2) min^{-1} or 158.5 L(H_2) min^{-1} g^{-1} (for the highest catalyst loading) were measured, which classify our catalyst among the most reactive ones. The NMR study showed a rapid NH_3BH_3 hydrolysis also at room temperature with initial formation of $B(OH)_4^-$, which besides would favor following equilibriums of formation of polyborates. Finally, after deactivation of the catalyst in the first run, the hydrolysis mechanism resulted substantially unmodified. These results are reported and discussed herein.

1. Introduction

One of the principal problems for the conversion to a viable hydrogen fuel economy is the development of on-board hydrogen storage materials with high gravimetric and volumetric hydrogen density. Various solutions are currently under investigation such as tanks of compressed and liquefied H_2, gas-on-solid adsorbents, metal hydrides (e.g., MgH_2, LiH, and $TiFeH_2$) and chemical complexes. In this last category, metal borohydrides (e.g., $LiBH_4$ and $NaBH_4$) and alanates (e.g., $NaAlH_4$) cover a central role; the high gravimetric hydrogen density (e.g., 18.4 wt% for $LiBH_4$) and the acceptable stability in aqueous alkaline solutions enable envisaging their utilization in on-board systems. However, the presence of solid by-products and the high costs needed for regeneration processes represent the principal obstacles for their extensive utilization [1].

Amineboranes, which are other examples of the attractive chemical complexes, have releasable protic (N–H) and hydridic (B–H) hydrogens. The parent ammonia borane, NH_3BH_3, with a very high hydrogen capacity (19.6 wt%), and low molecular weight (30.7 g mol^{-1}) represents a leading material for hydrogen storage applications [2,3] although the same problems above described for the adoption of chemical complexes in hydrolytic dehydrogenation routes were also found for amineboranes. Furthermore, a considerable disadvantage in automotive applications is the releasing of ammonia to the fuel cells, which requires additional precautions and gas clean-up. Dehydrogenation of NH_3BH_3 has been extensively analyzed in the solid state by thermolysis [4,5], and in solution by hydrolysis and methanolysis [6,7]. Recent studies have shown that metal-complexes-catalyzed dehydrogenation of NH_3BH_3 and substituted amineboranes enable a considerable extent of hydrogen release at affordable temperatures [8–10].

Ammonia borane shows a very good solubility in water [11]. In addition, it is highly stable in neutral and alkaline solutions as observed in ^{11}B NMR investigation [12,13] unlike $NaBH_4$, which undergoes self-hydrolysis. Besides solid acids [13], such as cation-exchange resins and zeolites, noble transition metal-based catalysts are extensively studied in NH_3BH_3 hydrolysis although their costs of utilization still represent a considerable drawback for a broad applicability [6,14–17]; it was reported that NH_3BH_3 is subjected to dissociation and hydrolysis in the presence of noble transition metal-based catalysts with a very high kinetics of hydrogen release [12]. Two different solutions may be adopted in order to mitigate their economical impact. They consist in the utilization

* Corresponding author. Tel.: +33 04 72 44 84 03; fax: +33 04 72 44 06 18.
E-mail address: umit.demirci@univ-lyon1.fr (U.B. Demirci).

0920-5861/$ – see front matter © 2011 Elsevier B.V. All rights reserved.
doi:10.1016/j.cattod.2011.01.040

of first-row transition metal-based catalysts, which are cheaper and more abundant (e.g., cobalt or nickel), and the modulation of the noble metal content maintaining the number of active sites through the reduction of the particle sizes. In both cases, the catalyst activates release of stored hydrogen up until 85 °C, which is the operative temperature for polymer exchange membrane fuel cells. Although many efforts were carried out in the attempt to develop efficient and economical accessible metal-based catalysts, the definition of the optimal compromise between costs and recyclability and the control of ammonia release during hydrolysis are still important challenges to overcome [18,19].

In the present study, supported ruthenium nanoparticles were generated by chemical reduction starting from an organometallic precursor. Small content (1.50 wt% as theoretical value) of ruthenium was dispersed over γ-Al_2O_3, which was chosen for its relatively high specific surface area and high stability in alkaline solutions. The catalyst was tested in hydrogen generation by NH_3BH_3 hydrolysis. The H_2 evolution was followed by water-displacement technique in combination with ^{11}B and $^{11}B\{^1H\}$ NMR that are utilized also for assessing the catalyst durability. Our main results are reported hereafter and discussed.

2. Experimental

2.1. General data

Reactions and workups were carried out under dry argon atmospheres using conventional Schlenk techniques unless noted. Ethylene glycol (Aldrich, 99+%), γ-Al_2O_3 (Evonik, AEROXIDE® Alu C, BET = 100 $m^2\ g^{-1}$), NH_3BH_3 (**1**, Aldrich, 97% and 90%), $Ru(C_4H_4O_2)_3$ (**2**, Strem, 99%), D_2O (Euriso-Top, 100%) were used as received. Ultrapure water with a specific resistance of 18.2 MΩ cm was obtained by a reverse osmosis followed by ion-exchange and filtration (PureLab Ultra, ELGA, USA) and used after purging with argon. The temperature of the solution in the reaction tube for the hydrolysis tests was recorded by a bayonet type-T (copper–constantan) thermocouple with a stainless steel sheath. The temperature of bath was controlled within ±0.1 °C by the thermostatic circulator.

^{11}B and $^{11}B\{^1H\}$ NMR spectra were recorded on Bruker 400 MHz FT spectrometers. The ^{11}B chemical shifts are given in δ_B units (parts per million) downfield from $BF_3{\cdot}O(C_2H_4)_2$ (δ_B = 0.0 ppm in $CDCl_3$). NMR spectra were taken through the investigation runs although the magnetic field homogeneity was systematically lowered by H_2 bubbling off. The phase structure of the catalyst was checked by powder X-ray diffraction (XRD) on a Bruker D5005 powder diffractometer (Cu Kα radiation, λ = 0.15406 nm). Transmission electron microscopy (TEM) analysis was performed on a Jeol 2010 LaB6 microscope equipped with an Oxford Instrument Link ISIS energy dispersive X-ray (EDX) spectrometer using an accelerating voltage of 200 kV. Scanning electron microscopy (SEM) was conducted on a Hitachi S-800 field emission gun (FEG) instrument at an acceleration voltage of 15–20 kV. The samples were sputtered with gold or a gold–palladium alloy.

Electronic and chemical states of the synthesized samples were characterized by X-ray photoelectron spectroscopy (XPS) on a Kratos Analytical Axis Ultra DLD spectrometer equipped with an Al Kα ($h\nu$ = 1486.6 eV, 150 W). The spectrometer binding energy (E_b) scale was calibrated using the position of Al 2p (74.0 eV) core level. The elaborations were performed using the commercial software Vision. The textural data of the catalysts were measured by N_2 adsorption at liquid N_2 temperature with a Sorptomatic 1990 – Thermo Electron instrument. The sample was degassed at 150 °C overnight before measurement. Elemental composition was determined by inductively coupled plasma (ICP) emission spectroscopy at the *Service Central d'Analyses du CNRS* at Vernaison, France.

2.2. Synthesis of the catalyst

In a two-necked round bottom flask, **2** (0.059 g, 0.000148 mol, 1.5 wt% of Ru) was dissolved in ethylene glycol (50.0 mL). The flask was evacuated under oil pump vacuum (2 min) without cooling and stirred at 185 °C (3 h). The resulting black slurry was cooled to 100 °C and γ-Al_2O_3 (0.985 g) was added under argon flow in one portion. After 12 h, the slurry was cooled to room temperature. The black precipitate was isolated by filtration, washed with ethanol (3× 20 mL), and dried by oil pump vacuum at 60 °C for 12 h to give ruthenium catalyst (Ru/γ-Al_2O_3, **3**) as a dark grey powder.

2.3. Hydrogen generation (typical procedure)

A 20 mL test tube was loaded in a glove box with **3** (0.0092 g, 10 wt%), and a magnetic stirring bar. The tube was sealed with a silicon septum, submerged in a preheated water bath to the desired reaction temperature using a thermostatic circulator, and connected to a water-filled inverted burette via a cold trap at −140 °C to ensure the water vapor and ammonia retainment. A second tube was loaded in a glove box with **1** (0.0850 g, 0.00275 mol) and sealed with a silicon septum. Distilled water (2.75 g) was added to the tube containing **1** with a syringe. The resulting solution was heated in a water bath at the desired temperature for 5 min before injection in the tube containing **3**. The evolved hydrogen was collected in a gas burette. The amount of collected hydrogen evolved was calculated using the ideal gas law. The experiments were recorded by a video camera connected to a computer. Data concerning hydrogen evolution were collected and analyzed using a Matlab program. Hydrogen generation rates (r) were then calculated.

2.4. ^{11}B and $^{11}B\{^1H\}$ NMR experiments

In a glove box, an NMR tube was charged with **3** (0.0058 g, 15 wt%). A solution of **1** (0.0327 g, 0.0011 mol) in D_2O (0.7 mL, C_1 = 1.6 M) was prepared in a 10 mL vial, cooled to −3 °C, and added via syringe under argon flow into the NMR tube containing **3**. ^{11}B and $^{11}B\{^1H\}$ NMR spectra were immediately recorded. The reaction was monitored at 25 °C at 20 min intervals. The NMR tube cap was provided with a small hole to relieve the pressure due to the hydrogen released during the experiment.

2.5. ^{11}B and $^{11}B\{^1H\}$ variable temperature (VT) NMR experiment

In a glove box, an NMR tube was charged with **3** (0.0034 g, 10 wt%). The tube was cooled to −3 °C. A solution of **1** (0.0309 g, 0.0010 mol) in D_2O (1.0 mL, C_1 = 1.0 M) was prepared in a 10 mL vial, cooled to −3 °C, and added via syringe under argon flow into the NMR tube containing **3**. The NMR tube was transferred to a 5 °C NMR probe after a brief shake. ^{11}B NMR spectra were recorded. The reaction was monitored at 15 °C intervals as the probe was warmed from 5 °C to 65 °C (heating rate of 3 °C min^{-1}). Before data acquisition, the sample was equilibrated for 3 min at each temperature. The NMR tube cap was provided with a small hole to relieve the pressure due to the hydrogen released during the experiment.

2.6. Analysis of Ru/γ-Al_2O_3 durability

In a glove box, an NMR tube was charged with **3** (0.0062 g, 20 wt%). A solution of **1** (0.0250 g, 0.000809 mol) in D_2O (0.6 mL, C_1 = 1.3 M) was prepared in a 10 mL vial, cooled to −3 °C, and added via syringe under argon flow into the NMR tube containing **3**. The NMR tube was cooled to −3 °C and transferred to a 65 °C NMR probe after a brief shake. ^{11}B and $^{11}B\{^{11}H\}$ NMR spectra were immediately recorded. The reaction was monitored at 7.5 min intervals. In each of following three runs, the supernatant in the NMR tube

was carefully recovered after the experiment under argon flow. The black precipitate was washed with D_2O (2× 1.0 mL) and combined again with **1** as above described. The reactions were monitored at 3 min intervals. The NMR tube cap was provided with a small hole to relieve the pressure due to the hydrogen released during the experiment.

3. Results and discussion

3.1. Catalyst characterization

Ethylene glycol was utilized as solvent and reducing agent for the synthesis of the catalyst [20–22]. It represents a material at lower environmental impact in comparison with other widely used reducing agents as $NaBH_4$, N_2H_4, CH_2O and DMF. Furthermore, it ensures mild temperature conditions and high solubility of **2**, which is adopted as metallic precursor. The complete incorporation of ruthenium evaluated by ICP (1.6 wt% *vs.* 1.5 wt% as theoretical value), represents a farther advantage. The specific area of **3** was determined by BET method. The utilization of ethylene glycol as solvent determines a contraction (76 $m^2\,g^{-1}$) with respect to the experimental value of γ-Al_2O_3 surface before synthesis (97 $m^2\,g^{-1}$); this relevant decreasing can be likely attributed to the partial blockage of the support porosity by ruthenium particles.

The morphology of **3** was analyzed by TEM and SEM. The first technique highlights the presence of spherical particles of variable sizes embedded on the outside area of the support (Fig. 1a). The particle size distribution is depicted in Fig. 2. An average particle size of 4.2 nm was determined. The contemporaneous formation of large-dimension aggregates (Fig. 1b) would confirm the difficulty to ensure an effective dimensional control of the particles in the presence of diols as reducing means [23,24]. The formation of large agglomerates through the back-scattered electron image is shown in SEM analysis (Fig. 3). This observation supports the relevant contraction (ca. 22%) of the surface area after synthesis of **3**.

The catalyst and support γ-Al_2O_3 (ICDD 00-050-0741) show analogous amorphous profile in the XRD diffraction patterns as illustrated in Fig. 4. In particular, the peaks of highest intensity of ruthenium (Ru with $2\theta = 44^\circ$; ICDD 00-001-1253) and ruthenium oxide (RuO_2 with $2\theta = 56^\circ$; ICDD 00-002-1365) were tracked. A very small peak centered at around $2\theta = 43^\circ$ is discernable and might be attributed to the ruthenium species. However, the low amount of the metallic component did not enable a farther exploitation of the XRD pattern.

XPS and EDX were utilized in order to investigate the composition of **3**. The former technique shows the presence of ruthenium at the catalyst surface. The ruthenium $3d_{5/2}$ and $3d_{3/2}$ binding energies (BEs) are diagnostic to confirm the presence of metallic ruthenium (Ru^0). The former BE, centered at 279.7 eV, indicates the presence of Ru^0 (Fig. 5) [25,26]. The latter one at 283.8 eV, covered by the signal of C 1 s, is consistent with BEs values related to Ru $3d_{3/2}$ [26]. Mathematical deconvolution provided the best fit of the experimental data assuming the presence of oxidized ruthenium. The ruthenium $3d_{5/2}$ BE value of 281.5 eV was found and ascribed to the oxide RuO_2 [26]. In summary, our catalyst appeared to consist of Ru^0 and RuO_2 supported over γ-Al_2O_3. Finally, strong peaks of ruthenium were observed by EDX analysis, which confirmed an effective deposition of metal particles at the surface of the support.

3.2. Hydrolysis followed by ^{11}B NMR and $^{11}B\{^1H\}$ NMR

The stability of **1** was monitored by ^{11}B NMR. Ammonia borane dissolves in water (33.6 g/100 g of H_2O) [2] and forms a colorless solution (pH = 9.1) [12]. ^{11}B NMR spectrum of **1** in D_2O exhibits a quartet centered at $\delta = -21.0$ ppm ($^1J_{BH} = 91.7$ Hz) in good agreement with previous reports [27,28]. The absence of modifications after 7 d, confirms the stability of **1** in aqueous solution at neutral pH (Fig. 6). Accordingly in the experiments detailed hereafter, the H_2 release can be attributed uniquely to the catalyst reactivity. ^{11}B NMR control experiment points out the inertness of the support γ-Al_2O_3 as shown in Fig. 7.

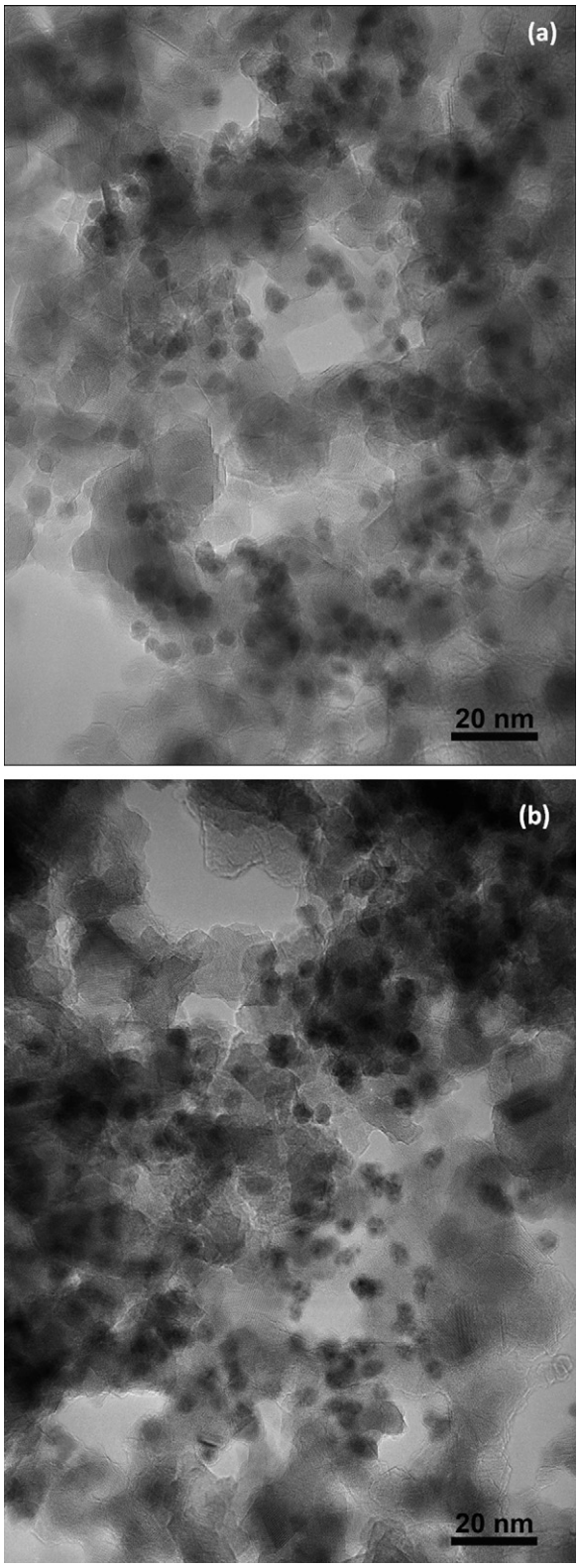

Fig. 1. TEM micrographs of **3**: (a) nanoparticles and (b) agglomerates.

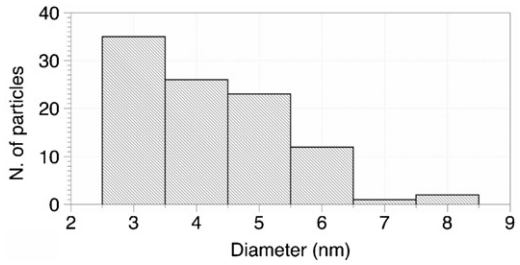

Fig. 2. Particle size distribution of **3**.

The hydrolytic dehydrogenation of **1** mediated by noble transition metal-based catalysts (e.g., Pt, Pd, or Ru) at standard conditions is reported as follows (Eq. (1)):

$$NH_3BH_3\,(aq) + 4H_2O\,(l) \rightarrow B(OH)_4^-\,(aq) + NH_4^+ + 3H_2\,(g) \quad (1)$$

The dehydrogenation of **1** in D_2O was monitored by VT ^{11}B NMR (Fig. 8). As the temperature was increased, the peak at −21.0 ppm of **1** progressively disappeared. A broad singlet showed up at lower field starting 50 °C (δ = 16.9 ppm at 65 °C), with no other signals being observed. According to the equation above, the singlet is ascribed to $B(OH)_4^-$. This suggests that NH_3BH_3 hydrolyzes into $B(OH)_4$-upon its adsorption over the catalyst surface, with no intermediates desorbing.

A farther test was performed in order to enucleate the reaction in Eq. (1). The hydrolytic dehydrogenation of **1** in the presence of **3** at room temperature was followed by $^{11}B\{^1H\}$ NMR as shown in Fig. 9. In this case, the broad peak at 9.8 ppm is assigned to a borate-adduct initially formed. In the attempt to account the observed ^{11}B NMR resonance, Chandra and Xu, report that an equilibrium process between H_3BO_3, BO_3^-, and other borate species would occur [12]. The signal was up-field shifted to 7.4 ppm after 2 h and, finally, to 6.4 ppm after 2 d. The chemical shift modification may be due to variations of pH and NH_4^+ concentration [29]. Moreover, a second broad peak had appeared after 2 d at higher chemical shift (9.5 ppm). The signal at 6.4 ppm is assigned to $B(OH)_4^-$ whereas the second one to a polyborate formed during the reaction; the presence of $B(OH)_4^-$ would favor the equilibriums of formation of polyborates in our operative conditions [29].

3.3. Hydrogen evolution

The rate of hydrogen release, expressed in $mL(H_2)\,min^{-1}$, was studied in the presence of **3** at 65 °C. This temperature was chosen with the aim to find the best compromise among: (i) the utilization of polymer electrolyte membrane fuel cells with operative temperatures lower than 85 °C; (ii) the time of hydrogen release (relatively fast measurements); (iii) the control of hydrogen release (smooth hydrogen evolution and absence of catalytic material loss within the exhaust lines).

Different approaches were utilized to study the hydrogen release processes in the presence of **3**. First, the effect of the concentration of **1** (1.0–0.65 M) was analyzed with the catalyst amount (10 wt%) and the temperature (65 °C) kept unchanged (Fig. 10). The rate of hydrogen release passes from 21.8 $mL(H_2)\,min^{-1}$ with the initial concentration of **1** (1.0 M) to 18.4 $mL(H_2)\,min^{-1}$ with the final one (0.65 M). The function $\ln(r) = f([NH_3BH_3])$ was plotted (not reported) to determine the reaction order with respect to the concentration of **1**. The rate law can be expressed as in Eq. (2):

$$r = \propto [NH_3BH_3]^{0.4} \quad (2)$$

The order 0.4 is quite consistent with that reported elsewhere for a 3 wt% Ru/C catalyst [30], namely 0.45. Basu et al. [30,31] suggested a Langmuir–Hinshelwood mechanism to capture such an order, which is also likely in our present conditions. It is noteworthy that zero-order kinetics has been reported, for e.g., supported Pt [6], Pd [32] and Co [33] catalysts. In fact, a discrepancy in the order *vs.* the hydride concentration has been also reported in the case of $NaBH_4$; it depends on the catalyst nature as well as the

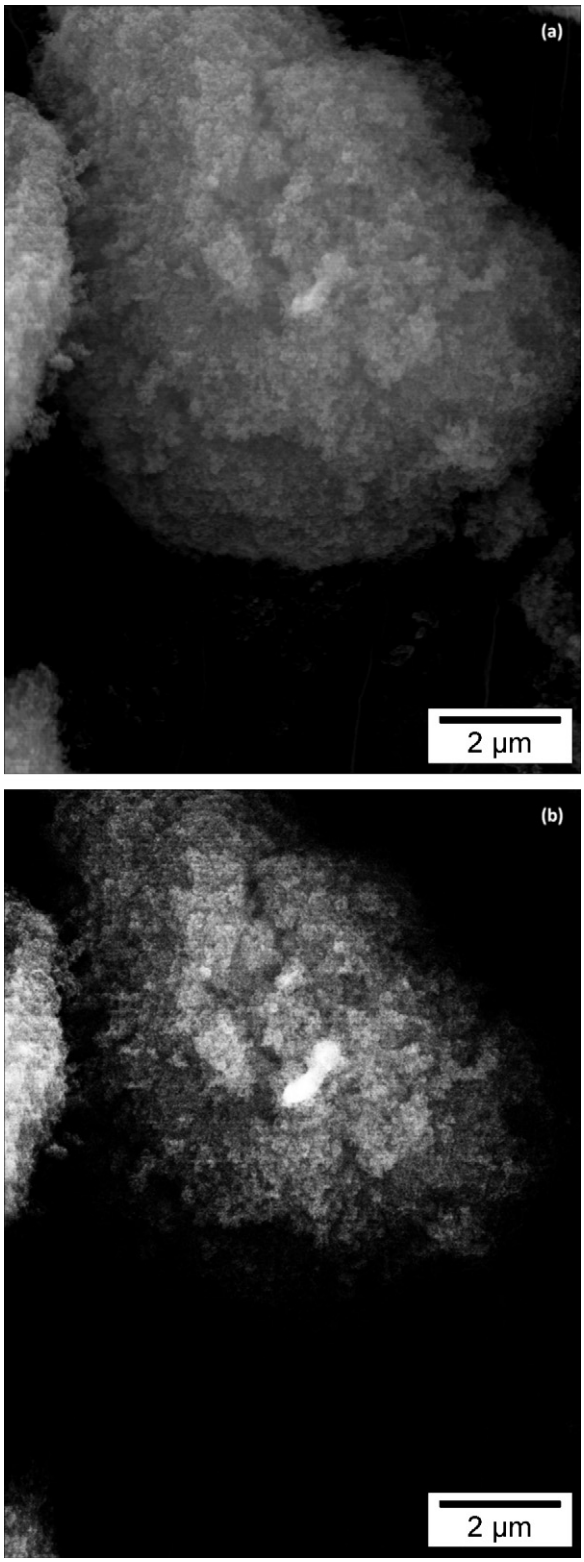

Fig. 3. SEM micrographs of **3** observed in secondary electrons (a) and back-scattered images (b).

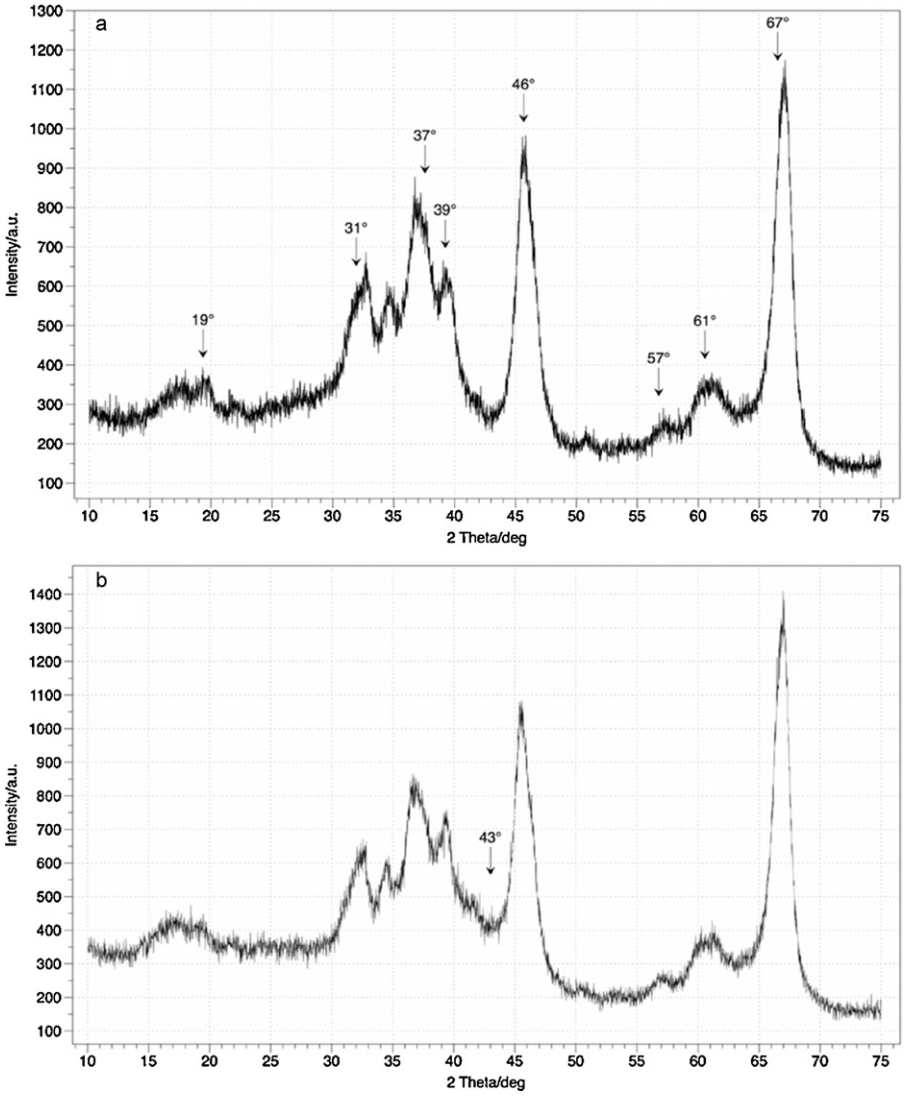

Fig. 4. XRD patterns of γ-Al_2O_3 (a) and **3** (b).

experimental conditions (mainly, hydride concentration range and temperature) [34].

Following tests were provided modifying the quantity of the catalyst (10–30 wt%) and leaving the concentration of **1** (1.0 M) as a constant (Fig. 11). The progressive increasing of the concentration of catalytically active surface sites of the ruthenium catalyst (θ_{Ru}) enabled a considerable improvement of the rate of hydrogen release, which passed from 17.8 mL(H_2) min^{-1} with the initial catalyst amount (10 wt%) to 76.4 mL(H_2) min^{-1} with the final one. For comparison purpose, one may report that Chandra and Xu [6] found a rate of 111 mL(H_2) min^{-1} at 40 °C for 2 wt% Ru/γ-Al_2O_3 (about 5 wt% with respect to NH_3BH_3) showing nanoparticles of 1.8 nm.

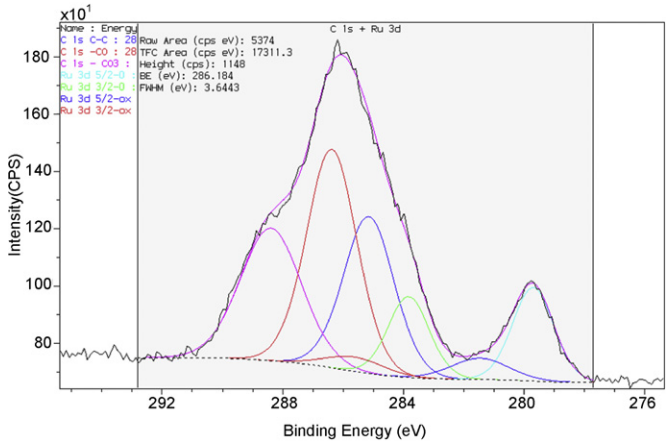

Fig. 5. Partial XPS spectrum of **3**. C 1s–Ru $3d_{5/2}$ levels for **3**.

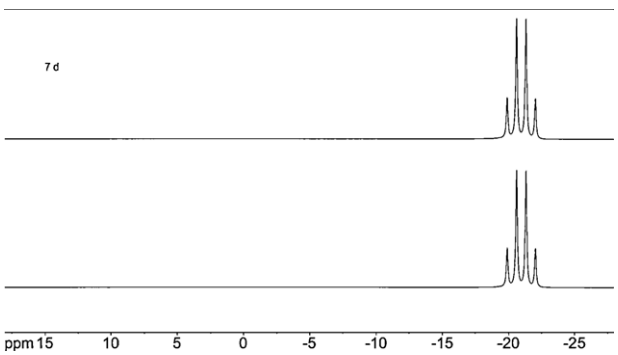

Fig. 6. ^{11}B NMR spectra of **1** (solvent: D_2O, C_1 = 1.3 M) after 5 min and 7 d.

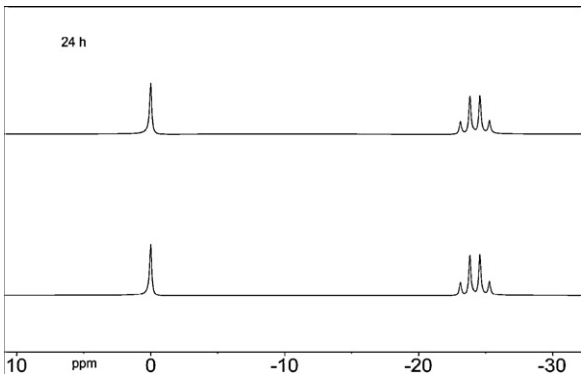

Fig. 7. $^{11}B\{^1H\}$NMR spectra of **1** in the presence uniquely of γ-Al_2O_3 (solvent: D_2O).

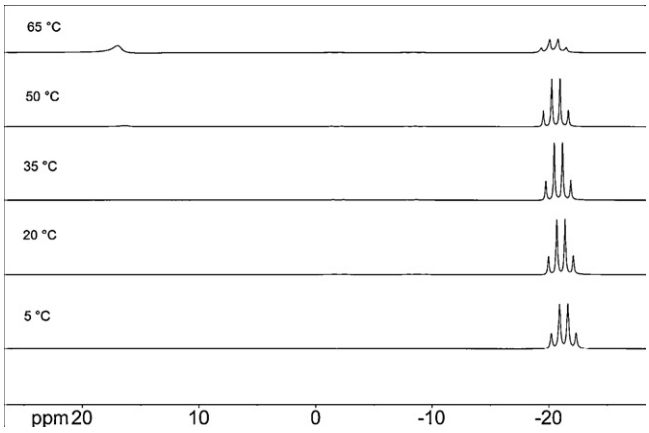

Fig. 8. VT ^{11}B NMR spectra of the hydrolytic dehydrogenation of **1**.

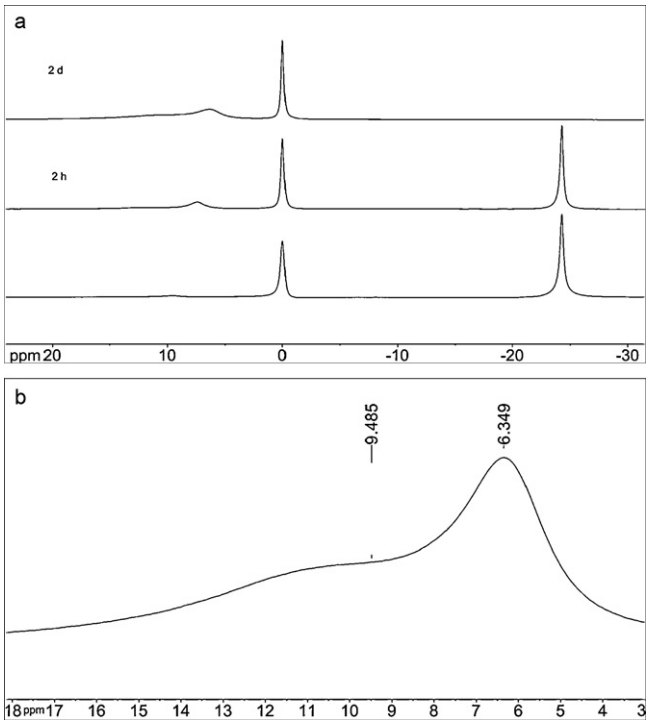

Fig. 9. $^{11}B\{^1H\}$ NMR spectra of the hydrolytic dehydrogenation of **1**; overall (a) and partial after 2 d (b). The first spectrum in (a) was recorded after 5 min.

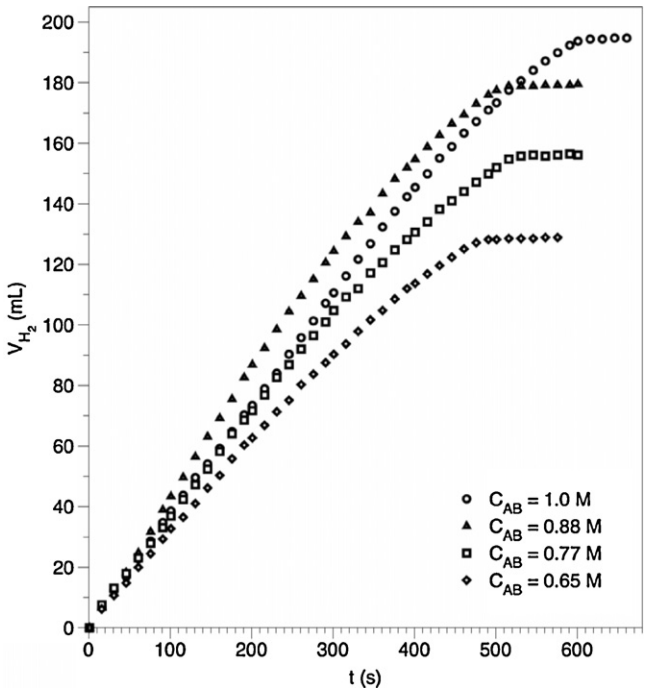

Fig. 10. Hydrogen release at different concentrations of **1**, with the catalyst amount (10 wt%) and temperature (65 °C) kept unchanged.

The function $\ln(r) = f(\theta_{Ru})$ was plotted (not reported) and the apparent order with respect to the concentration of catalytically active surface sites of the ruthenium catalyst was determined; it is shown in Eq. (3):

$$r \propto [\theta_{Ru}]^{1.0} \quad (3)$$

Such a reaction order is typical of catalytic processes.

The rates of hydrogen generation (from Fig. 11) were calculated also with respect to the catalyst amount and metal

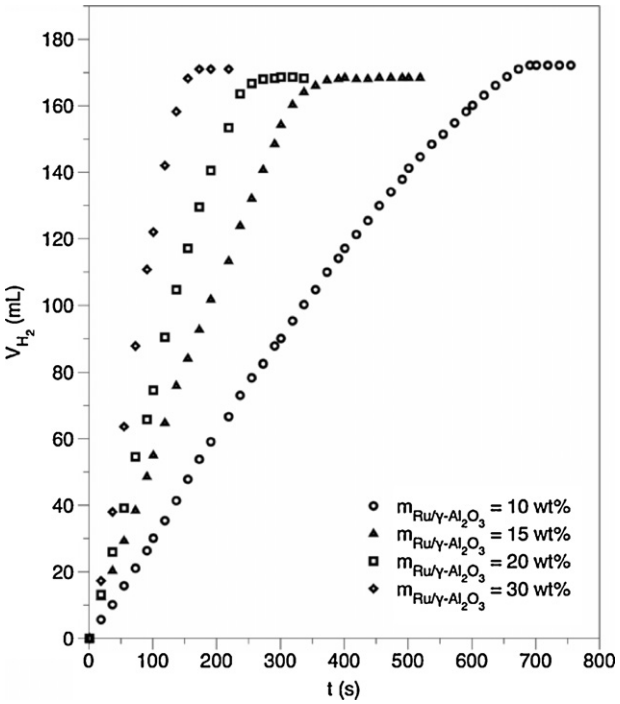

Fig. 11. Hydrogen release at different amount of **3**, with the concentration of **1** (1.0 M) and temperature (65 °C) kept unchanged.

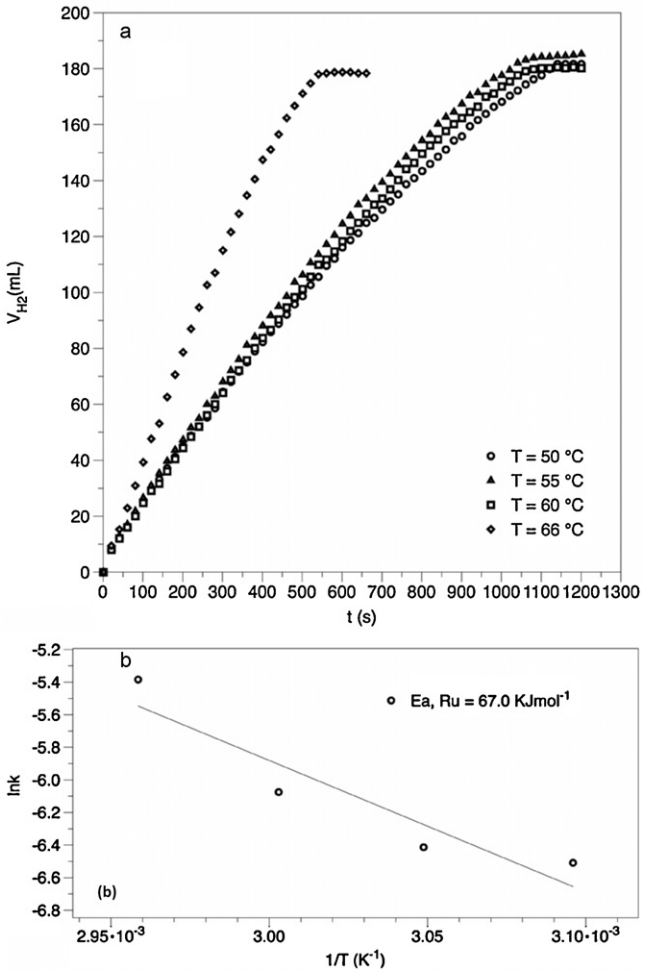

Fig. 12. Hydrogen release at different temperatures, with the catalyst amount (10 wt%) and concentration of **1** kept unchanged (1.0 M) (a), and Arrhenius plot for dehydrogenation of **1** (b).

content, with values of, respectively, 2.1 L(H_2) min^{-1} g^{-1} and 141.3 L(H_2) min^{-1} g^{-1} for the initial experiment, and 2.4 L(H_2) min^{-1} g^{-1} and 158.5 L(H_2) min^{-1} g^{-1} for the final one. These values confirm the high performance of our catalyst if correlated with other examples reported in the literature that belong to the same class of catalysts: e.g., 320 L(H_2) min^{-1} g^{-1} for 2 wt% Pt/γ-Al_2O_3 at 25 °C [6]; 210 L(H_2) min^{-1} g^{-1}(Rh) for 1.2 wt% Rh/zeolite-Y at 25 °C [35]; and 270 L(H_2) min^{-1} g^{-1} (Ru) for 3 wt% Ru/C at 55 °C [30].

The effect of the temperature was studied at constant values of the concentrations of **1** (1.0 M) and **3** (10 wt%) (Fig. 12a). The temperature was varied from 50 to 66 °C. The Arrhenius plot is reported in Fig. 12b. The apparent activation energy for **3** is 67 kJ mol^{-1}. Chandra and Xu reported a value of 23 kJ mol^{-1} in the presence of a similar Ru/γ-Al_2O_3 system [6]. Other analogous examples were reported, such as 76 kJ mol^{-1} with 3 wt% Ru/C [30]; 56 kJ mol^{-1} with intrazeolite Co^0 nanoclusters [33]; and 67 kJ mol^{-1} with 1.2 wt% Rh/zeolite-Y [35]. The difference may be attributed to the discrepancies introduced through the experimental procedures, such as differences in the utilized materials and experimental procedures. Note that the Arrhenius plot shows a downward curvature that might be indicative of a change in the mechanism of hydrolysis though our present data (especially NMR) does not support this.

To summarize, in our experimental conditions, the catalyst **3** obey a power rate law that shows an apparent activation energy of 67 kJ mol^{-1}, a reaction order *vs.* the NH_3BH_3 concentration of 0.4

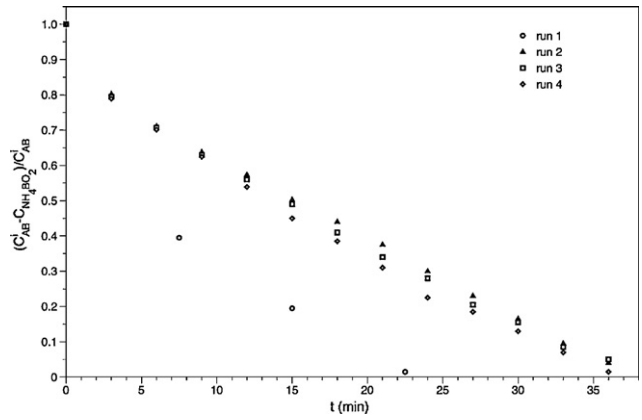

Fig. 13. Rates of hydrolytic dehydrogenation of **1** in successive runs (C^i_1 = 1.3 M; $m_{catalyst}$ = 20 wt%).

and an order *vs.* the concentration of catalytically active surface sites of the ruthenium catalyst of 1.0. This is consistent with the Langmuir–Hinshelwood mechanism [31,32], which supposes that both reactants, i.e. NH_3BH_3 and H_2O adsorb over the catalytic surface to be hydrolyzed upon the formation of the final by-product $B(OH)_4^-$. Furthermore, it suggests that the rate determining step is adsorption.

3.4. Catalyst durability

The catalyst durability was monitored by $^{11}B\{^1H\}$ NMR over four successive runs. The results, in terms of variation of the relative concentration of **1** during the time, are summarized in Fig. 13. The catalytic activity of **3** decreased after the first run. No further significant deactivation was observed for the remaining experiments (runs 2–4). The spectra recorded for run 1 and run 4 were com-

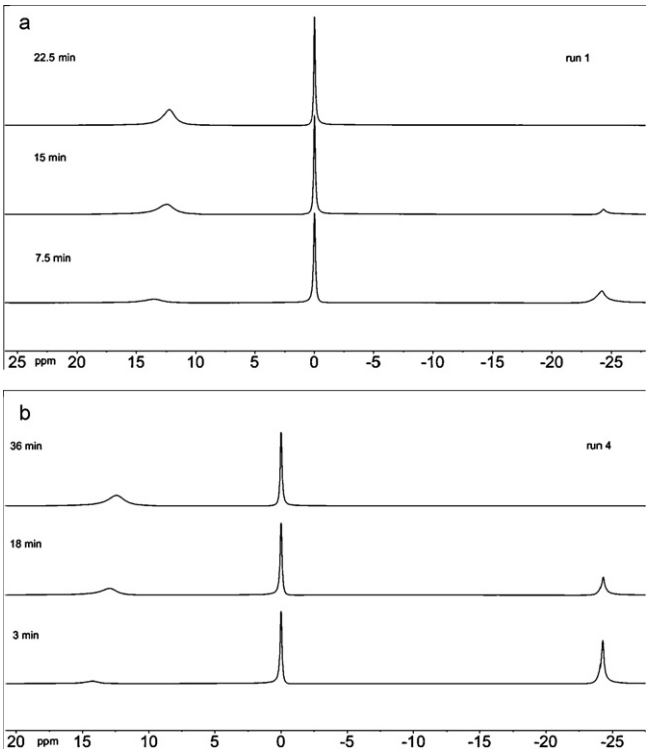

Fig. 14. $^{11}B\{^1H\}$ NMR spectra for the durability tests in the presence of **3**; run 1 (a) and run 4 (b).

pared; the catalytic behavior of **3**, in terms of resulting products, was identical along the experimental pathway (Fig. 14). A single product, i.e. $B(OH)_4^-$, was formed and, as observed above, its peak was slightly up-field shifted upon consumption of the substrate as function of solution features like the pH and borates concentration.

In our experimental conditions, the catalyst underwent deactivation after the first run. A plausible reason may be the precipitation of borates to the catalyst surface [36]. However, no further reduction of activity was observed in the following runs. In addition, the hydrolysis mechanisms appeared to remain unchanged since the activity of 3, was identical along the successive runs. This behavior resembles the properties of cobalt-based catalysts used in $NaBH_4$ hydrolysis [37]. In order to rationalize the previous outcomes, it is proposed that the catalyst underwent a substantial modification of ruthenium species at the surface through an *in situ* reduction promoted by 1. After the first run, the surface of **3** is presumably uniform and characterized by the preponderant presence of Ru^0, which would represent the stable phase as the spectral results of runs 2–4 confirm. Further experiments are thus required to highlight this but, to succeed in this, the *in situ* characterizations issue must be addressed; this is a complicated challenge [37].

4. Conclusion

A highly active supported catalyst, 1.5 wt% $Ru/\gamma\text{-}Al_2O_3$, for hydrolytic dehydrogenation of NH_3BH_3 was synthesized by chemical reduction using an effective polyol methodology. By ICP and XPS, it was found that the catalyst consisted of 1.6 wt% Ru^0 and RuO_2. By SEM and TEM, it was observed that the nanoparticles with an average diameter of 4.2 nm were rather aggregated and deposited over the surface of $\gamma\text{-}Al_2O_3$; this was confirmed by N_2 adsorption/desorption and EDX measurements.

The reactivity of the catalyst was tested at various concentrations of NH_3BH_3, catalyst contents, and temperatures. It is noteworthy that, as reported elsewhere, NH_3 releases while NH_3BH_3 is hydrolyzing; this is one of the most significant drawbacks the process faces. In the present study, NH_3 was trapped in the cold trap and the proportion of NH_3 was below 20 ppm in the H_2 stream. A specific study is in progress to assess the amount of NH_3 released in various experimental conditions. Compared to other liquid-phase hydrogen generation reactions [38] such as hydrolysis of $LiBH_4$ or $NaBH_4$, this issue is detrimental to the implementation of NH_3BH_3 hydrolysis; compared to hydrogen generation from hydrous hydrazine, which side-reaction generates NH_3, hydrolysis of NH_3BH_3 is of interest as long as a 100% selectivity in H_2 is not achieved in the former case. However that may be, all of these processes are under investigation and each shows to have potential for technological applications.

A kinetic study was thus conducted and the power rate low to which $Ru/\gamma\text{-}Al_2O_3$ obeys was determined. The apparent activation energy was found to be 67 kJ mol^{-1}. The order *vs*. the NH_3BH_3 concentration was 0.4 and the order *vs*. the concentration of Ru active surface sites 1.0. Such data are quite consistent with some reported so far. Furthermore, high hydrogen generation rates were measured in the first run, which classify our catalyst among the most reactive ones. The catalyst suffered from deactivation after the first run but its reactivity was maintained for subsequent runs. On-going studies are addressed to improve the catalyst durability and costs by combination of ruthenium species with cheaper and more abundant first-row transition metals, such as cobalt and copper.

Mechanistic insights gained by ^{11}B NMR analysis offer the possibility to propose few considerations as follows: (i) the catalytic inertness of $\gamma\text{-}Al_2O_3$ was confirmed in our operative conditions; (ii) the initial product of the reaction is $B(OH)_4^-$; no B–N adducts or intermediates were detected during the reaction; (iii) the presence of $B(OH)_4^-$ would favor equilibriums of formation, post-hydrolysis, of additional borate species, assumed to be polyborates; (iv) the catalytic behavior of $Ru/\gamma\text{-}Al_2O_3$ is identical along the experimental pathway despite a deactivation after a first run. These observations combined together with those from the kinetic study are consisted with a heterogeneous catalysis following the Langmuir–Hinshelwood mechanism.

Acknowledgments

This research was supported by the *Agence Nationale de la Recherche* – France (BoraHCx project). The authors thank Ms. Caroline Toppan from the *École Supérieure de Chimie Physique Électronique – Université Claude Bernard Lyon 1* for her assistance in the NMR experiments.

References

[1] U. Eberle, M. Felderhoff, F. Schüth, Angew. Chem., Int. Ed. 48 (2009) 6608.
[2] F.H. Stephens, V. Pons, R.T. Baker, Dalton Trans. 25 (2007) 2613.
[3] B. Peng, J. Chen, Energy Environ. Sci. 1 (2008) 479.
[4] V. Hu, R.A. Geanangel, W.W. Wendlandt, Thermochim. Acta 23 (1978) 249.
[5] G. Wolf, J. Baumann, F. Baitalow, F.P. Hoffmann, Thermochim. Acta 343 (2000) 19.
[6] M. Chandra, Q. Xu, J. Power Sources 168 (2007) 135.
[7] P.V. Ramachandran, P.D. Gagare, Inorg. Chem. 46 (2007) 7810.
[8] C.A. Jaska, K. Temple, A.J. Lough, I. Manners, J. Am. Chem. Soc. 125 (2003) 9424.
[9] M.C. Denney, V. Pons, T.J. Hebden, D.M. Heinekey, K.I. Goldberg, J. Am. Chem. Soc. 128 (2006) 12048.
[10] Y. Kawano, M. Urichi, M. Shimoi, S. Taki, T. Kawaguchi, T. Kakizawa, H. Ogino, J. Am. Chem. Soc. 131 (2009) 14946.
[11] A.T. Raissi, Proceedings of the 2002. U.S. DOE Hydrogen Program Review, http://www.eere.energy.gov/hydrogenandfuelcells/pdfs/32405b15.pdf.
[12] M. Chandra, Q. Xu, J. Power Sources 156 (2006) 190.
[13] M. Chandra, Q. Xu, J. Power Sources 159 (2006) 855.
[14] T.J. Clark, G.R. Whittell, I. Manners, Inorg. Chem. 46 (2007) 7522.
[15] J.M. Yan, X.B. Zang, S. Han, H. Shioyama, Q. Xu, Angew. Chem., Int. Ed. 47 (2008) 2287.
[16] S.B. Kalindindi, M. Indirani, B.R. Jagirdar, Inorg. Chem. 47 (2008) 7424.
[17] F. Durap, M. Zahmakiran, S. Özkar, Appl. Catal. A 369 (2009) 53.
[18] U.B. Demirci, P. Miele, Energy Environ. Sci. 2 (2009) 627.
[19] U.B. Demirci, S. Bernard, R. Chiriac, F. Toche, P. Miele, J. Power Sources 196 (2011) 279.
[20] S. Sun, C.B. Murray, D. Weller, L. Folks, A. Moser, Science 287 (2000) 1989.
[21] J. Sun, J. Kim, Y. Hou, C. Wang, Angew. Chem., Int. Ed. 46 (2007) 6333.
[22] R.D. Rutledge, W.H. Morris, M.S. Wellons, Z. Gai, J. Shen, J. Bentley, J.E. Wittig, C.M. Lukehart, J. Am. Chem. Soc. 128 (2006) 14210.
[23] I. Pastoriza-Santos, L.M. Liz-Marzan, Nano Lett. 2 (2002) 165.
[24] H. Zeng, J. Li, Z.L. Wang, J.P. Liu, Nano Lett. 4 (2004) 187.
[25] C.D. Wagner, W.M. Riggs, L.E. Davis, J.F. Moulder, G.E. Mullenberg, Handbook of X-Ray Photoelectron Spectroscopy, Perkin-Elmer Corporation, Physical Electronics Revision, Eden Prairie, MN 55344, 1979, and references therein.
[26] NIST XPS Database, http://srdata.nist.gov/xps/Default.aspx, and references therein.
[27] D.F. Gaines, R. Schaeffer, J. Am. Chem. Soc. 86 (1964) 1505.
[28] C.W. Heitsch, Inorg. Chem. 4 (1965) 1019.
[29] C.G. Salentine, Inorg. Chem. 22 (1983) 3920.
[30] S. Basu, A. Brockman, P. Gagare, Y. Zheng, P.V. Ramachandran, W.N. Delgass, J.P. Gore, J. Power Sources 188 (2009) 238.
[31] S. Basu, Y. Zheng, A. Varma, W.N. Delgass, J.P. Gore, J. Power Sources 195 (2010) 1957.
[32] M. Rakap, S. Özkar, Int. J. Hydrogen Energy 35 (2010) 1305.
[33] M. Rakap, S. Özkar, Int. J. Hydrogen Energy 35 (2010) 3341.
[34] U.B. Demirci, O. Akdim, J. Andrieux, J. Hannauer, R. Chamoun, P. Miele, Fuel Cells 10 (2010) 335.
[35] M. Zahmakiran, S. Özkar, Appl. Catal. B 89 (2009) 104.
[36] S.C. Amendola, S.L. Sharp-Goldman, M.N. Saleem Janjua, C. Spencer, M.T. Kelly, P.J. Petillo, M. Binder, Int. J. Hydrogen Energy 25 (2000) 969.
[37] U.B. Demirci, P. Miele, Phys. Chem. Chem. Phys. (2010), doi:10.1039/C0CP00295J.
[38] H.L. Jiang, S.K. Singh, J.M. Yan, X.B. Zhang, Q. Xu, Chem. Sus. Chem. 3 (2010) 541.